INTERNAL SOLAR ROTATION

TAKASHI SEKII
Institute of Astronomy, University of Cambridge
Madingley Road, Cambridge CB3 0HA, UK

1. Introduction

The rotation of the sun affects the wave propagation in the solar cavity. The measurement of the effect can be used to infer the internal rotation of the sun, and indeed much of what we know today about the dynamics of the solar interior has been derived from observation and interpretation of the rotationally induced splitting of solar p-mode frequencies. Inversion has proven to be a very powerful tool in such investigations, and will remain at the centre of our effort in studying solar rotation from helioseimic data. Study of the flow inside the sun is not only important in its own right but is vital for improving our understanding of solar activity and its cycle. Now that both GONG and SOHO are operational and are accumulating data, there is no doubt that we are about to learn a great deal more about the dynamical structure of our own star.

In this review various inversion techniques, specifically in the context of the rotation inversion, are discussed. Then, what we have learned so far is summarized, and results from the latest observations are discussed, particularly those from the GONG experiment (Harvey *et al.* 1996).

2. Rotational splitting

Normal modes of the sun, a three-dimensional body, are identified by three indices: radial order n, spherical harmonic degree l and azimuthal order m. In the absence of any symmetry-breaking agent, the eigenfrequency has $(2l+1)$-fold degeneracy in m. The solar rotation breaks the spherical symmetry and lifts this degeneracy, causing the frequency to split into $2l+1$ different values. Let us describe rotation by the two-dimensional distribution of angular velocity $\Omega(r,\mu)$, where r is the radial coordinate and μ is the cosine of the colatitude θ. By treating rotation as a perturbation to a spherically symmetric sun, and by applying linear perturbation theory, we obtain

$$\Delta\omega_{nlm} \equiv \omega_{nlm} - \omega_{nl} = m\langle\Omega\rangle_{nlm} \ , \tag{1}$$

where ω_{nlm} is the frequency in the presence of the rotation, ω_{nl} is the unperturbed degenerate frequency and $\langle\Omega\rangle_{nlm}$ denotes a weighted integral of angular velocity $\Omega(r,\mu)$:

$$\langle\Omega\rangle_{nlm} = \frac{\Delta\Omega_{nlm}}{m} = \int_0^R dr \int_{-1}^1 d\mu K_{nlm}(r,\mu)\Omega(r,\mu) \ , \tag{2}$$

where $K_{nlm}(r,\mu)$ is the splitting kernel for the mode under consideration, representing the extent to which $\Omega(r,\mu)$ influences this particular mode. Observationally, $\langle\Omega\rangle_{nlm}/\omega_{nl} \sim 0.5\mu\text{Hz}/3\text{mHz} \sim 10^{-4}$, and this justifies the application of linear perturbation theory. Our aim is, given a set of observations of rotational splitting, $\{\Delta\omega_{nlm}\}$, to solve the corresponding set of linear integral equations (2) for the angular velocity $\Omega(r,\mu)$.

There is more than one way to write down $K_{nlm}(r,\mu)$ explicitly (e.g., Hansen, Cox and van Horn 1971), but the following is convenient in presenting the mathematical structure:

$$K_{nlm}(r,\mu) = K_{nl}(r)W_{lm}(\mu) + L_{nl}(r)X_{lm}(\mu) \ , \tag{3}$$

where

$$K_{ln}(r) = (\xi_r^2 + \{l(l+1)-1\}\xi_h^2 - 2\xi_r\xi_h)\rho r^2/I_{ln} \tag{4}$$
$$L_{ln}(r) = \xi_h^2\rho r^2/I_{ln} \tag{5}$$
$$W_{lm}(\mu) = P_l^m(\mu)^2 \tag{6}$$
$$X_{lm}(\mu) = \frac{d}{d\mu}\left[\frac{1-\mu^2}{2}\frac{d}{d\mu}W_{lm}(\mu) + \mu W_{lm}(\mu)\right] \tag{7}$$
$$I_{ln} = \int [\xi_r^2 + l(l+1)\xi_h^2]\rho r^2 dr \ , \tag{8}$$

ρ is density, P_l^m is a normalized associated Legendre function and ξ_r and ξ_h determine the radial and horizontal components of the radial part of the displacement vector $\boldsymbol{\xi}_{nlm}$ according to

$$\boldsymbol{\xi}_{nlm} = \left[\ \xi_r(r),\ \xi_h(r)\frac{\partial}{\partial\theta},\ \xi_h(r)\frac{1}{\sin\theta}\frac{\partial}{\partial\phi}\ \right] P_l^m(\cos\theta)e^{im\phi-\omega_{nlm}t} \ , \tag{9}$$

with respect to spherical polar coordinates (r,θ,ϕ). Some examples of the splitting kernels are shown in Figure 1.

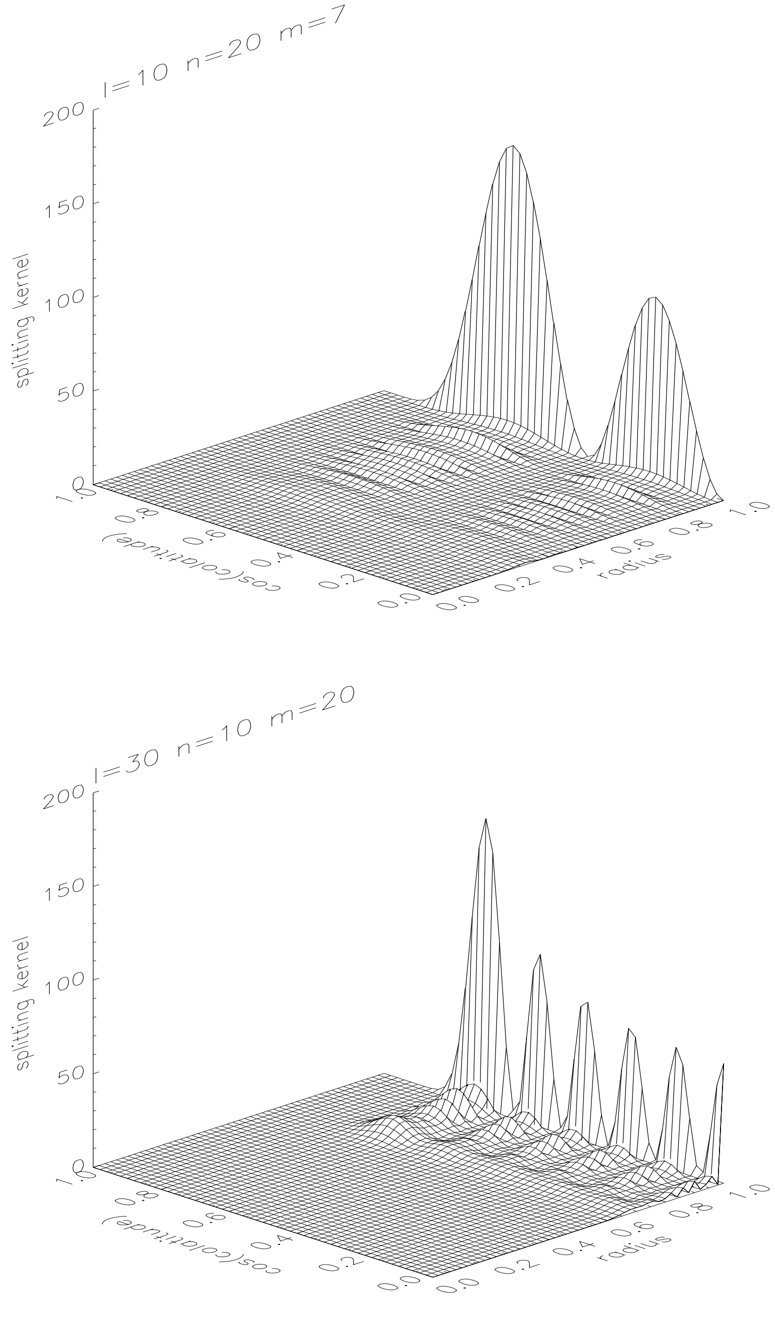

Figure 1. Some examples of the splitting kernels, represented as surface plots against r, the radial coordinate, and μ, the cosine of the colatitude. $(l, n, m) = (10, 20, 7)$ [top] and $(30, 10, 20)$ [bottom].

From the above expression one notes that the kernel $K_{nlm}(r,\mu)$ is degenerate. Moreover, for high-order p modes, except near the inner turning point, ξ_r dominates over ξ_h, and hence

$$K_{nlm}(r,\mu) \simeq K_{nl}(r) W_{lm}(\mu) \ . \tag{10}$$

This property is noticeable in Figure 1.

Also, the angular parts of the kernel, $W_{lm}(\mu)$ and $X_{lm}(\mu)$, are even functions of μ, regardless of the value of m. This means that the kernel always samples the northern and the southern hemisphere equally. As a result, within the linear regime, we can never measure the north-south asymmetry of the angular velocity.

Finally, the integral of $X_{lm}(\mu)$ vanishes. Therefore, for a one-dimensional case, where $\Omega(r,\mu) = \Omega(r)$, we have

$$\Delta\omega_{nl} = \int_0^R K_{nl}(r)\Omega(r)dr \ , \tag{11}$$

where $\Delta\omega_{nl} \equiv \Delta\omega_{nll}/l$.

3. Inversion of solar p-mode rotational-splitting data

Since most of the fundamental aspects of inversion do not depend on the dimension of the space in which the problem is posed, for simplicity the one-dimensional inversion of constraints (11), for a given set of $\{\Delta\omega_{nl}\}$, is considered in this section. There are two important classes of methods of obtaining estimates of $\Omega(r)$: optimally localized averaging (Backus and Gilbert 1968, 1970) and regularized least-squares fitting (Phillips 1962, Twomey 1963, Tikhonov 1963). Both methods give linear estimates of the angular velocity; the estimate of Ω at a certain radius r_0, $\hat{\Omega}(r_0)$, is a linear combination of the observations $\{\Delta\omega_{nl}\}$. Thus we may write

$$\hat{\Omega}(r_0) = \sum_{nl} c_{nl}(r_0)\Delta\omega_{nl} = \int_0^R D(r;r_0)\Omega(r)dr \ , \tag{12}$$

where

$$D(r;r_0) \equiv \sum_{nl} c_{nl}(r_0) K_{nl}(r) \tag{13}$$

is the *averaging kernel*. The coefficients $c_{nl}(r_0)$ are called inversion coefficients at the target radius r_0. To discuss the error in the estimate, in general we should consider the the error covariance matrix of $\Delta\omega_{nl}$ (*e.g.*, Gough 1996). Once again for simplicity, however, let us assume that the errors are independent and the matrix is diagonal. Then the standard deviation in the estimate $\hat{\Omega}(r_0)$ is given by

$$\delta\hat{\Omega}(r_0) = \left(\sum_{nl} c_{nl}(r_0)^2 \sigma_{nl}^2 \right)^{1/2} , \tag{14}$$

where σ_{nl} is the standard deviation of $\Delta\omega_{nl}$.

3.1. OPTIMALLY LOCALIZED AVERAGING (OLA)

The basic idea of optimally localized averaging (OLA) is readily explained by equations (12) – (14). Since we would like $\hat{\Omega}(r_0)$ to be as close as possible to $\Omega(r)$, we would like the averaging kernel $D(r; r_0)$ to be well localized. However, the more one localizes $D(r; r_0)$, usually the greater is the amplitude of the coefficients $c_{nl}(r_0)$, and hence the greater error in the estimate: a trade-off between resolution and error must be sought.

In OLA one seeks a balance by minimizing, *e.g.*,

$$S \equiv \int D(r; r_0)^2 (r - r_0)^2 dr + \alpha \sum_{nl} c_{nl}^2 \sigma_{nl}^2 , \tag{15}$$

subject to the unimodular condition

$$\int_0^R D(r; r_0) dr = 1 , \tag{16}$$

where α is a regularization parameter which controls the trade-off.

An important variant of the standard OLA described above is the subtractive optimally localized averaging (SOLA) in the form considered by Pijpers and Thompson (1992). In SOLA one attempts to fit $D(r; r_0)$ to a prescribed function such as a Gaussian centred at a target radius with an appropriate width.

3.2. REGULARIZED LEAST-SQUARES FITTING (RLS)

In regularized least-squares fitting (RLS), one seeks to fit the data by minimizing

$$S = \sum_{nl} \frac{1}{\sigma_{nl}^2} \left[\Delta\omega_{nl} - \int_0^R K_{nl}(r)\Omega(r) dr \right]^2 + \alpha \int_0^R [\mathcal{L}\Omega(r)]^2 dr , \tag{17}$$

where α is again a regularization parameter and $\mathcal{L}$ is, say, a differential operator that measures the 'smoothness' of $\Omega(r)$, or some other property that one might wish to optimize. Minimization of S leads to another integral

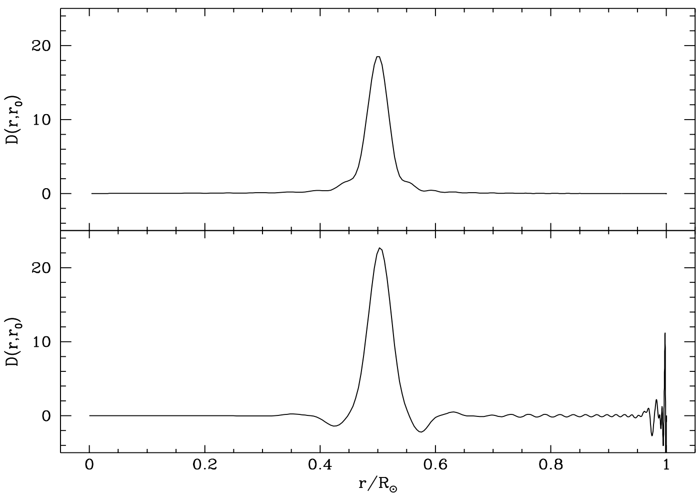

Figure 2. Examples of averaging kernel for $r_0 = 0.5$, obtained by an OLA inversion (top) and an RLS inversion (bottom). The mode set is identical to the GONG Hare-and-Hound exercise (Gough and Toomre 1993).

equation that involves the adjoint of $\mathcal{L}$, which one might solve by expanding $\Omega(r)$ in a series of functions. Usually, however, the expansion is carried out before the minimization. Either way, it can be shown that we can still write the estimate of $\Omega(r)$ at a certain radius r_0 as a linear combination of the data in the manner of equation (12).

Had the regularization term not been included, in the case of solar p modes the minimization of S would require the inversion of a nearly singular matrix producing an 'ill-posed problem', and the solution would typically contain spurious highly oscillatory components which are generated by numerical and data errors. This is due to the fact that all the splitting kernels have large amplitude near the surface with a large amount of redundancy in the information that the datasets carry.

3.3. COMPARISON BETWEEN OLA AND RLS

Helioseismologists have been using both OLA and RLS for their inversions. Between the two methods, OLA gives better localization, because the method is designed that way. Figure 2 compares typical averaging kernels produced from an OLA inversion and from a RLS inversion. The OLA averaging kernel has almost no sidelobes and no surface contamination, both of which are undesirable. Depending on the mode set, even OLA kernels can have these features, but to a much less extent than the RLS kernels. As was pointed out by Christensen-Dalsgaard, Schou and Thompson (1990), however, the negative sidelobes can contribute to improve the estimate. For example, if $\Omega(r)$ is convex (or concave) in the region where the averaging is taking place, the localized average by a positive definite kernel would underestimate (or overestimate) $\Omega(r)$, but negative sidelobes push up (or down) the estimate, provided that the averaging kernel stays unimodular. This is what the regularization term does: interpolation and extrapolation. Part of the side lobes therefore maybe accounted for as a designed property of RLS methods. Still, OLA gives better averaging kernels overall, and estimates that are more robust and more easily interpretable.

On the other hand, RLS is more responsive to internal inconsistency of the data, if it exists. Since an OLA method is concerned only about localization, it is left to helioseismologists to check the consistency of the data, but a RLS method directly looks at the misfit, and therefore such inconsistency, including ones arising from underestimating random errors, will show up immediately.

RLS is computationally cheaper, too. An OLA inversion involves inverting a matrix of size M, where M is the number of modes, per target point. If one needs to estimate $\Omega(r)$ on N_T target points, this takes $\sim M^3 N_T$ flops. RLS involves inverting a matrix of size N, where N is the number of functions in the expansion, or, in many cases, the number of grid points. So this takes $\sim N^3$ flops. If $M = 1000$, $N = 500$ and $N_T = 100$, then the ratio of the operation count is ~ 800. For a two-dimensional case, this ratio increases. For $M = 10^5$, $N = 5000$ and $N_T = 1000$, the ratio is $\sim 8 \times 10^6$.

In spite of these differences, in the real cases in helioseismology, OLA and RLS are usually in general agreement (see Figure 4, next section). However, this does not mean that the difference between the two is merely an operational one. To make this point, let us consider a linear equation

$$A\boldsymbol{x} = \boldsymbol{b} \ , \tag{18}$$

where A is an $m \times n$ matrix, and $\boldsymbol{x}$ and $\boldsymbol{b}$ are vectors of size n and m, respectively. From this one obtains $\hat{\boldsymbol{x}}$, an estimate of $\boldsymbol{x}$, as

$$\hat{\boldsymbol{x}} = R\boldsymbol{b} \ . \tag{19}$$

The resolution matrix R depends on the method one chooses to obtain the estimate. The estimate $\hat{\boldsymbol{x}}$ is related to the real solution $\boldsymbol{x}$ through the following formula (hence the name 'resolution' matrix)

$$\hat{\boldsymbol{x}} = R\boldsymbol{b} = RA\boldsymbol{x} \ , \tag{20}$$

while the vector of misfit is given by

$$\boldsymbol{b} - A\hat{\boldsymbol{x}} = (I_m - AR)\boldsymbol{b} \ , \tag{21}$$

where I_m is the identity matrix of size m. In the absence of data errors, OLA seeks to choose R in such a way that RA is as close as possible to I_n, the identity matrix of size n:

$$RA \to I_n \ . \tag{22}$$

On the other hand, RLS seeks to reduce the misfit and therefore aim to achieve

$$AR \to I_m \ . \tag{23}$$

We may write, therefore,

$$R_{\mathrm{OLA}} \simeq A_{\mathrm{L}}^{-1} \ , \quad R_{\mathrm{RLS}} \simeq A_{\mathrm{R}}^{-1} \ , \tag{24}$$

where R_{OLA} and R_{RLS} are the resolution matrices obtained from an OLA and an RLS inversion, respectively, and A_{L}^{-1} and A_{R}^{-1} denote the left and the right inverses. This suggests the fundamental difference and the complementary nature of OLA methods and RLS methods. It also means that these two classes of methods are not simply the ones we *happen* to know, but that they are *the* two fundamental bases.

We know from linear algebra that if one of either the right or the left inverse exists, then the other inverse exists, too, and they are identical. In this sense, the general agreement between the two inverses in helioseismic inversions is another indication that what we have been doing is not too far off the mark.

4. Inversions in two dimensions

Before GONG, measurement of individual splittings ω_{nlm} were not available. Instead, it was customary to expand the splittings in the form

$$\frac{\Delta\omega_{nlm}}{2\pi} = \sum_k a_k(n,l)\mathcal{P}_k(m;l) \ ,$$

where $\mathcal{P}_k(m;l)$ is some polynomial and a_k is an expansion coefficient. Ritzwoller and Lavely (1991) pointed out that it is advantageous to choose polynomials $\mathcal{P}_k(m;l)$ that are orthogonal in the discrete space of m. In any case, inversions of expansion coefficients normally reduce to inverting each set of expansion coefficients (at fixed k), which are one-dimensional inversions, and then combining them together.

Mathematically, inference of two-dimensional rotation, $\Omega(r,\theta)$, from individual splitting frequencies $\Delta\omega_{nlm}$, is no different from inference in one dimension. Computationally, however, it is much harder. With the number of modes of the order of 10^5, a straightforward application of OLA is prohibitively expensive. This was the reason the first two-dimensional inversions

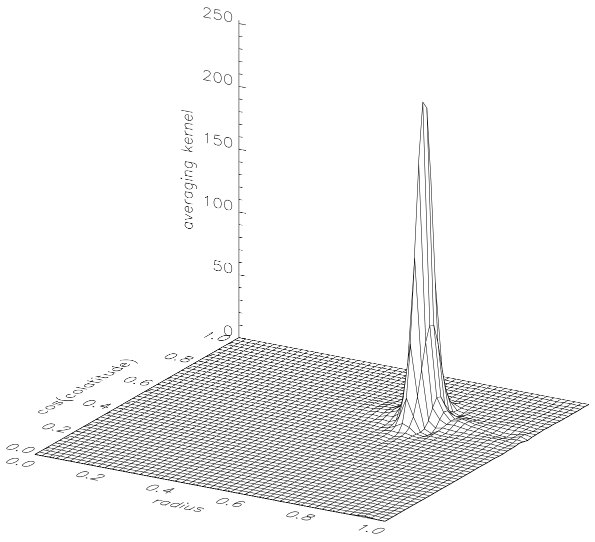

Figure 3. Surface plot of an averaging kernel obtained by a 1D⊗1D OLA inversion, centred at $r = 0.7R_\odot$, $\mu = 1/\sqrt{2}$.

were RLS inversions (*e.g.* Sekii 1990, 1991; Schou 1991, also Corbard *et al.* 1995)

A fully two-dimensional OLA was presented by Christensen-Dalsgaard *et al.* (1995). To invert a huge matrix they carried out singular-value decomposition and then truncated the spectral expansion to reduce the size of the problem. However, singular-value decomposition itself is a computationally intensive procedure, and therefore a fully two-dimensional OLA remains an extremely expensive method.

Sekii (1993a) pointed out that a property of the splitting kernels of the solar p-modes (equation 10) can be exploited to decompose the two-dimensional problem into successive one-dimensional inversions (1D⊗1D inversions). The sun's spherical geometry introduces a complexity, as was discussed by Sekii (1993b), but this decomposition still reduces the computational labour substantially, and it is possible to formulate OLA methods on this basis (Sekii 1993b, 1995; Pijpers & Thompson 1996).

An example of an averaging kernel obtained by this method is shown in Figure 3.

5. What we have learned

What we know today about the internal rotation of the sun, from observations of the past and the present, and from various analysis of them, are

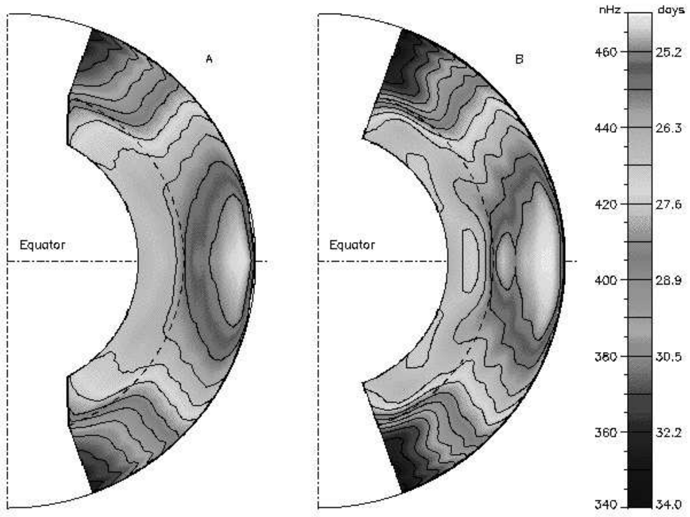

Figure 4. Rotation rate in the sun inferred from GONG data, by a 1D⊗1D OLA inversion (left) and by a 2D RLS inversion (right). From Thompson *et al.* (1996).

summarized as follows:

- the latitudinal variation of the angular velocity observed at the surface more-or-less persists throughout the convection zone,
- there appears to be weak differential rotation in the radiative interior,
- the maximum of the angular velocity occurs at $r/R_\odot \simeq 0.95$ (unless we have a rapidly spinning core!),
- there is suspected a shear layer immediately beneath the surface,
- there is a shear layer beneath the base of the convection zone.

Such features are seen in the inversions shown in Figure 4 (Thompson *et al.* 1996), obtained from 4 months of GONG data, and are in agreement with the LOWL result (Tomczyk, Schou and Thompson 1995), the latest GONG result (Korzennik *et al.* 1996) and the MDI result (Kosovichev *et al.* 1996).

A 1D⊗1D OLA inversion of the latest GONG data (Korzennik *et al.* 1996) is shown in Figures 5 and 6. The result is consistent with those shown in Figure 4. To investigate the structure below the base of the convection zone specifically, Douglas Gough and I have carried out a nonlinear least-squares fitting. (Figure 7). An analytical model of the rotation rate, comprising a rigidly rotating interior and a differentially rotating outer layer (latitudinal dependence is independent of radius), with a transition zone between them, is fitted in the least-squares sense to the GONG data. One

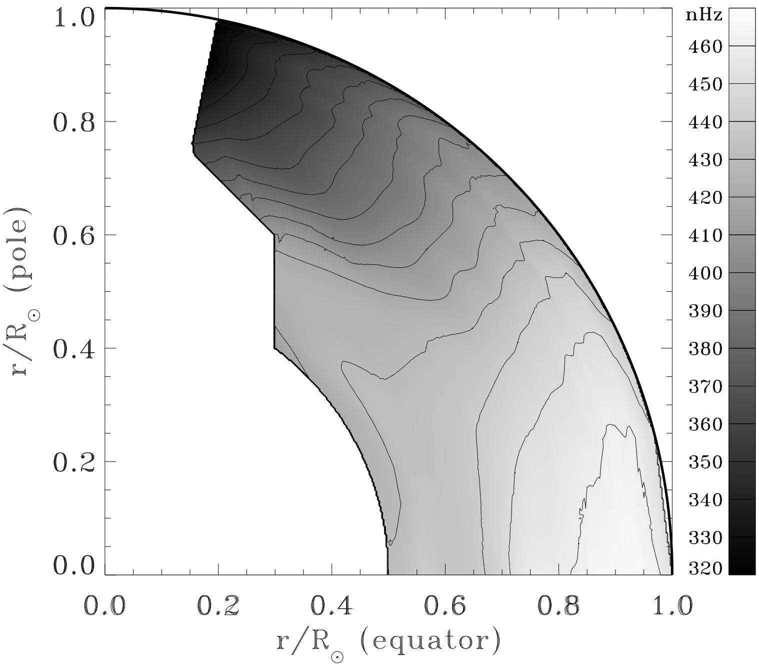

Figure 5. Contour diagram of a 1D⊗1D OLA inversion of the latest GONG data (Korzennik *et al.* 1996).

might note that the positions of the upper and the lower boundaries of the transition zone are nonlinearly related to the measurements, and that the fitting is accomplished by iteration. Please compare the result with that shown in Figure 6. The result indicates that the zone is centred at $r = 0.696R_{\odot}$, and the thickness of the zone is $0.064R_{\odot}$. Such a transition zone, known as a tachocline, was suggested to be a site of turbulent mixing by Spiegel and Zahn (1992) (cf. Gough and Sekii 1996).

Finally, an inversion in deeper layers was attempted (Figure 8). The averaging kernel is well localized, and the result suggests a rate slower than the surface value. This agrees with BiSON (Chaplin *et al.* 1996) and LOWL but not IRIS (Lazrek *et al.* 1996).

6. Future problems

In spite of our long efforts, the kinematics in the core remains largely uncertain.

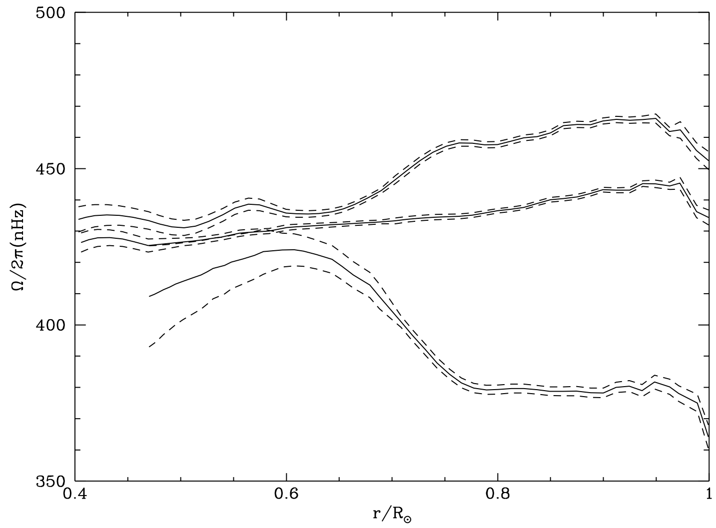

Figure 6. Rotation rate shown in Figure 5 are plotted as function of r at the latitudes of 0° (top), 30° (middle) and 60° (bottom). The dashed curves indicate error levels.

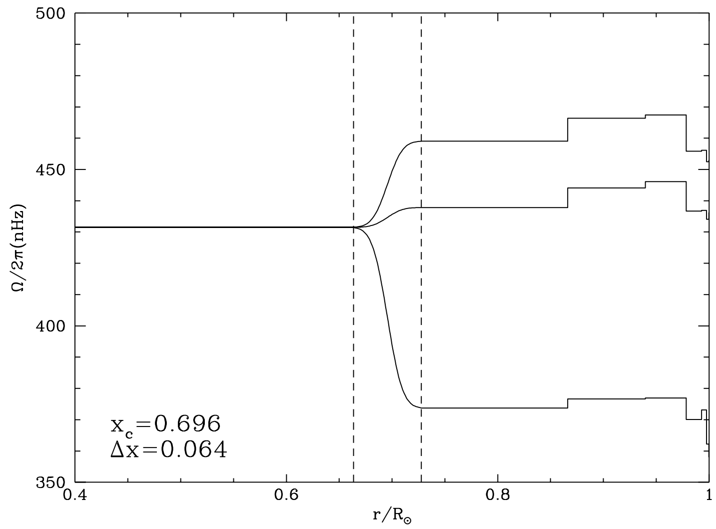

Figure 7. Result of a nonlinear least-squares fitting to the latest GONG data (Korzennik *et al.* 1996). Rotation rates at the latitudes of 0° (top), 30° (middle) and 60° (bottom) are obtained from fitting an analytic expression to the data. The transition zone is found to be centred at $r = 0.696R_\odot$ with a thickness $\Delta r = 0.064R_\odot$. The vertical dashed lines indicate the position of the upper and the lower boundaries.

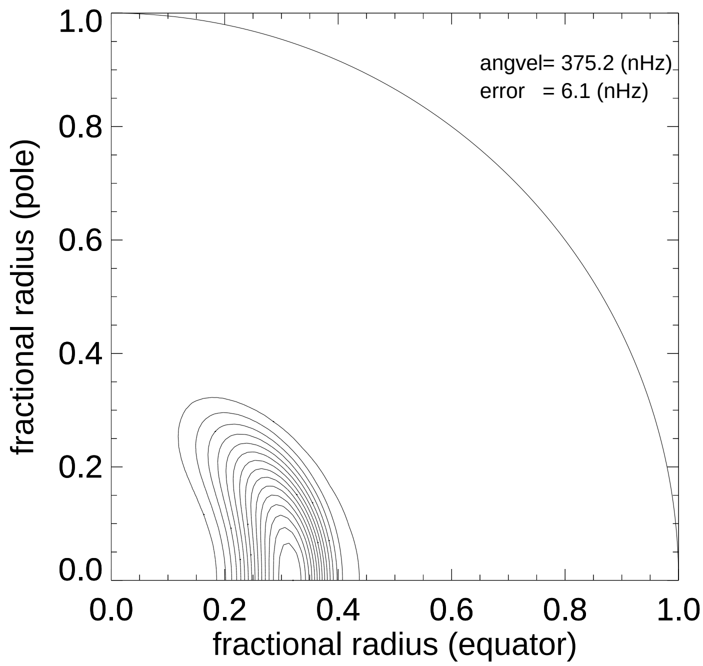

Figure 8. An averaging kernel obtained from a 1D⊗1D OLA inversion of the latest GONG data (Korzennik *et al.* 1996. The estimated rotation rate is $\Omega/2\pi = 375.2 \pm 6.1$(nHz).

The low-degree splitting measurement is a key to the issue, but observations are still not in mutual agreement, as was discussed by Pallé (1996). The disagreement may be coming from the difference in data analysis procedures, which shows how difficult such tasks indeed are (cf. Chang, Gough and Sekii 1996). G-modes, if found, would play an extremely important role in our investigation of the core. The helioseismic instruments on SOHO, as they accumulate more data, might solve both problems.

A new method of investigating the dynamics of solar interior is now developing. Local-helioseismological approaches do not rely on frequency splitting as such, but on measuring the travel times of acoustic waves in the sun between various parts of the solar surface. Inferences concerning the internal flow in three dimensions have been made (Kosovichev and Duvall 1996, Duvall *et al.* 1996). It is still unclear how deep down into the solar interior such an approach is effective, but this is certainly an exciting new tool in helioseismology that enables us to investigate the dynamics of the outer layer in great detail.

References

1. Backus, G. and Gilbert, F. 1968, *Geophys. J. Roy. Astron. Soc.* **16**, 169
2. Backus, G. and Gilbert, F. 1970, *Phil. Trans. Roy. Soc. London, Ser. A* **266**, 123
3. Chang, H.-Y., Gough, D.O. and Sekii, T. 1996, these proceedings
4. Chaplin, W.J., Elsworth, Y., Howe, R., Isaak, G.R., McLeod, C.P., Miller, B.A. and New, R. 1996, *MNRAS* **280**, 849
5. Christensen-Dalsgaard, J., Schou and Thompson, M.J. 1990, *MNRAS* **242**, 353
6. Christensen-Dalsgaard, J., Larsen, R.M., Schou and Thompson, M.J. 1995, in *GONG 1994: Helio- and Astero-Seismology from Earth and Space*, the Conference Series of the Astronomical Society of the Pacific, ed R. K. Ulrich (the Astronomical Society of the Pacific, San Francisco), 70
7. Corbard, T., Berthomieu, G., Gonczi, G., Provost, J. and Morel, P. 1995, in *The 4th SOHO Workshop, Helioseismology*, ed. B. Battrick (ESA Publication Division, Noordwijk), 289
8. Duvall, T.L., Jr. *et al.* 1996, these proceedings
9. Gough, D.O. 1996, in *The Structure of the Sun*, ed T. Roca Cortés (Cambridge University Press), 141
10. Gough, D.O. and Toomre, J. 1993, *GONG Report No. 11*
11. Gough, D.O. and Sekii, T. 1996, these proceedings
12. Hansen, C.J., Cox, J.P. and van Horn, H.M. 1977, *ApJ* **217**, 151
13. Harvey, J.W. *et al.* 1996, *Science* **272**, 1284
14. Korzennik, S.G., Thompson, M.J., Toomre, J. and the GONG internal rotation team 1996, these proceedings
15. Kosovichev, A.G. and Duvall, T.L., Jr. 1996, in *Solar Convection and Oscillations and their Relationship* eds. F.P. Pijpers, J. Christensen-Dalsgaard and C.S. Rosenthal (Kluwer Academic), in press
16. Kosovichev, A.G. *et al.* 1996, *Sol. Phys.*, submitted
17. Lazrek, M *et al.* 1996, *Sol. Phys.*, **166**, 1
18. Pallé, P.L. 1996, these proceedings
19. Phillips, D.L. 1962, *J.Ass.Comput. Mach.* **9**, 84
20. Pijpers, F.P. and Thompson, M.J. 1992, *A&A* **262**, L33
21. Pijpers, F.P. and Thompson, M.J. 1996, *MNRAS* **279**, 498
22. Ritzwoller, M.H. and Lavely, E.M. 1991, *ApJ* **369**, 557
23. Schou, J. 1991, in *Challenges to theories of the structure of moderate-mass stars*, eds. D.O. Gough and J. Toomre (Springer, Heidelberg)
24. Sekii, T. 1990, in *Progress of Seismology of the Sun and Stars*, eds. Y. Osaki and H. Shibahashi (Springer-Verlag, Berlin), 337
25. Sekii, T. 1991, *PASJ*, **43**, 381
26. Sekii, T. 1993a, in *GONG1992: Seismic Investigation of the Sun and Stars*, the Conference Series of the Astronomical Society of the Pacific, ed T.M. Brown (the Astronomical Society of the Pacific, San Francisco), 237
27. Sekii, T. 1993b, *MNRAS* **264**, 1018
28. Sekii, T. 1995, in *The 4th SOHO Workshop, Helioseismology*, ed. B. Battrick (ESA Publication Division, Noordwijk), 285
29. Spiegel, E.A. and Zahn, J.-P. 1992, *A&A*, **265**, 106
30. Thompson, M.J. *el al* 1996, *Science* **272**, 1300
31. Tomczyk, S., Schou, J. and Thompson, M.J. 1995, *ApJ*, L57
32. Tikhonov, A.N., 1963, *Sov. Maths-Dokl.* **4**, 1035
33. Twomey, S. 1963, *J. Ass. Comput. Mach.* **10**, 97